IJST, Transactions of Civil Engineering, Vol. 39, No. C1, pp 183-200
Printed in The Islamic Republic of Iran, 2015

THE PROPERTIES OF SCALE EFFECT ON THE DENSITY OF ROCKFILL MATERIALS BASED ON FRACTAL THEORY*

L. WU[1**], S. ZHU[2], Y. WANG[3], C. LU[4] AND S. DEND[5]

[1, 2,4,5]State Key Laboratory of Hydrology-water Resources and Hydraulic Eng., Hohai University, Nanjing, Jiangsu 210098, China
Email: 309027933@qq.com
[1,2,4,5]Institute of Hydraulic Structures, Hohai University, Nanjing, Jiangsu 210098, China
[3]HydroChina Huadong Engineering Corporation, Hangzhou, Zhejiang, 310014, China

Abstract– To study the scale effect on the density of rockfill materials, the relative density tests were carried out by physical tests and numerical tests. Fractal theory was drawn into the grading of rockfill materials. Then, the fractal properties of scale effect on the density were studied by physical tests and numerical tests. There are close relations between fractal dimension D and densities of rockfill materials. The densities are largest when D is the critical value D_c. Further, D_c is independent of the relative density D_r and the maximum diameter d_{max}. *Truncation error* is one of the main factors of scale effect of densities of rockfill materials. The existing four scale methods in the standard can all be explained with fractal theory, and a unified formula was suggested. The achievements in the paper lay a good foundation for further studying scale effect of rockfill materials with fractal theory.

Keywords– Scale effect, density, rockfill material, fractal theory, PFC2D (Particle Flow Code in 2 dimension)

1. INTRODUCTION

In recent years, more and more high earth-rockfill dams have been built and designed, particularly concrete faced rockfill dams (Yang *et al.*, 2011) [1]. Although the domestic damming technology is one of the leading technologies worldwide, there are still some engineering problems in the high rockfill dams (Xu *et al.*, 2008) [2]. Researchers have done a great deal of works on these problems [3-8]. However, there are no solutions in some problems such as scale effect in the rockfills. Scale effect is defined as the differences of physical and mechanical properties between indoor tests and field tests. In recent years, high rockfill dams have been springing up. The maximum diameters of dam materials are often between 600mm and 800mm, and sometimes up to 1200mm. However, the maximum diameter is only 60mm in most indoor tests. As a result, oversized particles must be removed and scale effect occurs.

The earliest study on scale effect was made by Bishop and Henkel [9]. There are two branches of the study on scale effect. One is the research on test apparatus [10-12]. The purpose is to weaken scale effect by widening the dimensions of the instrument. However, with the increasing dimensions of the instruments, the difficulty of servo-controlling on the confining pressure is increasing and the test costs are increasing, so the research was limited and the branch is progressing slowly. In contrast, the other branch which is focused on the disciplines between scale effect and characteristic diameter has shown promising results. Researchers [13-15] concluded that internal friction angle φ is decreasing while E_s and d_{max} are increasing. Some [16-18] considered that d_{max} has little influence on shear strength but much influence on deformation. Hennes [18] found that φ is increasing as the weighted average diameter d_0 as increases. Li [20] and Yang *et al.* [21] discovered that dynamic shear strength and dynamic shear modulus are

*Received by the editors March 19, 2013; Accepted March 4, 2014.
**Corresponding author

increasing while d_{max} is decreasing. From the above, we can see that there hasn't been a consensus on the scale effect. The reason is that the materials, the scale method and the densities are all not consistent, especially the densities. Weng [22] confirmed that scale effect on the density exists regardless of the four scale methods. However, more effort should be made to study the scale effect on the density more comprehensively.

Fractal theory is a new subject relative to Euclidean geometry theory. However, it has been widely applied to many fields for depicting the complex natural phenomena [23-28]. Turcotte [29] applied fractal geometry theory to geotechnical field. Tyler [30] proposed the formula of grading with fractal geometry theory. Yang *et al*. [31] and Zhu *et al*. [32] verified the gradings of soils and rockfill materials both satisfy fractal theory respectively.

In this paper, scale effect on the density was studied by physical and numerical tests. For the first time, the fractal properties of scale effect on the density were investigated, and the existing scale methods were analyzed from the view of fractal theory. In the end, a unified formula for scale method was suggested which relates fractal theory to scale effect. The achievements in the paper lay a good foundation for further studying scale effect of rockfill materials by fractal theory.

2. THEORY

Fragmentation plays an important role in various geological phenomena. Rocks are fragmented by joints and weathering. Explosives are often used to fragment rocks. Impacts produce fragmented ejecta. Statistical relations have been used to correlate data to the size distribution of fragments. A simple power law relation is often used, which is by definition a fractal. The concept provides a means of quantifying these processes which are various scale invariant processes in nature.

The size distribution of materials plays an important role in predicting physical and mechanical properties. One area of interest to scientists is the potential of fractal scaling in the particle-size distributions. In a PSD (particle-size distribution), the concept of fractal scaling suggests that across a wide range of scales, the solid phase of the material will appear to be similar (self-similarity). For a PSD with fractal scale, the volume $V(r > R)$ of cubes of size R needed to fill the grains of size R or larger is given by [33]:

$$V\left(r > R\right) = C_m \left[1 - \left(\frac{R}{\lambda_m}\right)^{3-D}\right] \tag{1}$$

where C_m and λ_m are constants describing shape and scale; D is fractal dimension.

However, Eq. (1) is generally not used when investigating the fractal behavior of PSDs. Instead, it appears to be more appropriate in terms of mass, which is more easily measured. From Eq. (1), the mass $M\left(r > R\right)$ is:

$$M\left(r > R\right) = \rho_p V = \rho_p C_m \left[1 - \left(\frac{R}{\lambda_{\mathrm{m}}}\right)^{3-D}\right] \tag{2}$$

where ρ_p is the grain density. Here, ρ_p is assumed to be independent of grain size. Thus, the total mass, M_T, is:

$$\begin{aligned} M_T &= M\left(r > 0\right) = \rho_p V \\ &= \rho_p C_m \left[1 - \left(\frac{0}{\lambda_{\mathrm{m}}}\right)^{3-D}\right] = \rho_p C_m \end{aligned} \tag{3}$$

And, Eq. (2) can be normalized by Eq. (3) to yield:

$$\frac{M\left(r>R\right)}{M_T}=1-\left(\frac{R}{\lambda_m}\right)^{3-D} \tag{4}$$

We chose R_L as upper size limit. Obviously, at $R = R_L$, $M\left(r>R\right)/M_T=0$. As a result, λ_m must be equivalent to R_L. Eq. (4) can be rewritten as:

$$\frac{M\left(r>R\right)}{M_T}=1-\left(\frac{R}{R_L}\right)^{3-D} \tag{5}$$

or

$$\frac{M\left(r<R\right)}{M_T}=\left(\frac{R}{R_L}\right)^{3-D} \tag{6}$$

In the geotechnical field, a PSD is usually determined by sieve analysis, so Eq. (6) is substituted by

$$p_i=100\left(\frac{d_i}{d_{\max}}\right)^{3-D} \tag{7}$$

where p_i is mass percentage, $p_i=100\times\frac{M\left(r<R\right)}{M_T}$; d_i is sieve diameter; $d_{\max}$ is the maximum diameter in a PSD.

Equation (7) is also called *Talbot curve*, which has been widely used in rockfill grading design. Studies have shown that rockfills with fractal grading can be compacted more easily.

3. TEST PROGRESS

a) Applicability and parameters

In this paper, PFC2D (Particle Flow Code in 2 dimension) was used to simulate geotechnical tests. Confining pressure dependence, dilatancy, nonlinearity, elastoplasticity and strength criterion are typical features of geotechnical materials. In the following, the four basic features of geotechnical materials were simulated, and the applicability of PFC2D was discussed. Then parameters of PFC2D were determined.

1. The simulation of triaxial compression tests

Triaxial compression tests are mostly used to determine the shear strength of geotechnical materials. The stress situation is axisymmetric, that is $\sigma_2=\sigma_3$. However, PFC2D is a 2-D software, so the simulated tests are called biaxial compression tests. The following assumptions are made for stress and strains in the third direction: Only two force components and one moment component exist in a PFC2D model, as opposed to the three force components and three moment components that exist in a three-dimensional particle assembly; the out-of-plane force component and the two in-plane moment components are not considered in any way in the equations of motion or in the force-displacement laws. Although the stress situations between triaxial compression tests and biaxial compression tests are not exactly the same, the qualitative properties of the two are consistent. The stress situations are shown in the following figure.

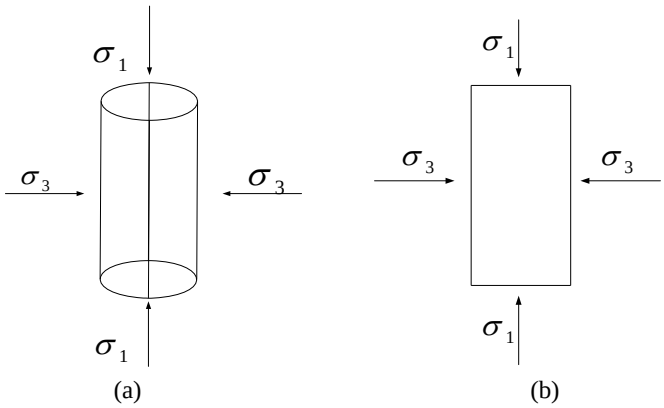

Fig. 1. The stress situations
(a) the triaxial test; (b) the biaxial test

In the triaxial test, the deviatoric stress is $\sigma_1 - \sigma_3$; the confining stress is σ_3; the volumetric strain is $\varepsilon_v = \varepsilon_1 + \varepsilon_2 + \varepsilon_3$. In the biaxial test, the deviatoric stress is $\sigma_1 - \sigma_3$; the confining stress is σ_3; the volumetric strain is $\varepsilon_v = \varepsilon_1 + \varepsilon_2 = \varepsilon_x + \varepsilon_y$. The main difference is the volumetric strain. In the 2D space, the strain in the third direction $\varepsilon_3 = 0$, is similar to plane strain situation. In this paper, the main purpose is to study qualitative properties of rockfill materials. The qualitative disciplines is enough, which can be confirmed in Fig. 9. The physical test is triaxial test and the numerical test is biaxial test. From the figure, we can see that the simulation method of biaxial tests used in the paper can reflect the laws of the stress-strain properties of triaxial tests.

2. Confining pressure dependence

Duncan-Chang Model was proposed based on conventional triaxial compression tests. The model has been validated and widely applied to geotechnical materials, so the model is a valid index for verifying the validity of PFC2D. The stress-strain curve is hyperbola, that is:

$$\sigma_1 - \sigma_3 = \frac{\varepsilon_1}{a + b\varepsilon_1} \tag{8}$$

Equation (8) can be translated to:

$$\frac{\varepsilon_1}{\sigma_1 - \sigma_3} = a + b\varepsilon_1 \tag{9}$$

Take $\frac{\varepsilon_1}{\sigma_1 - \sigma_3}$ as Y-axis and ε_1 as X-axis, Eq. (9) becomes linear, which is convenient to carry regression analysis. This is shown in Fig. 2b. The purpose of Fig. 2b is to investigate the agreement between the stress-strain curve and hyperbola under different confining pressures. Figure 2 shows that the stress-strain curves before the maximum values of $\sigma_1 - \sigma_3$ fitted well to hyperbola. The reason of disagreement after the maximum values of $\sigma_1 - \sigma_3$ is the absence of particle breakage.

Confining pressure is one of the most important factors. The shear strength increases with the increasing of the confining pressure. Figure 2 is the result of the conventional triaxial test simulated with PFC2D. In Fig. 2a, the curves decrease when ε_1 is larger than one value, which is not completely consistent with the results of physical test. Not taking particle breakage into consideration is the main reason. However, particle breakage is not the focus in the paper, so the results of Fig. 2a are expected and reasonable. In Fig. 2b, the test data were fitted to Duncan-Chang Model, which has been widely applied to geotechnical materials. From the picture, we can see that the fitting is well satisfied. The deviation appearing in the latter is due to not considering particle breakage. In a word, conventional triaxial test can be mechanically simulated with PFC2D.

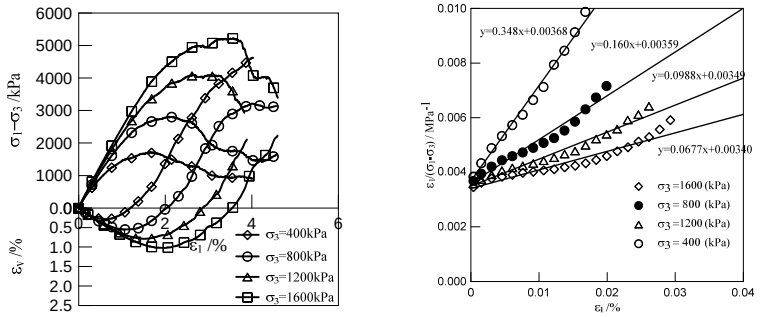

(a) (b)

Fig. 2. The stress-strain curve of the rockfills simulated with PFC2D
(a) The stress-strain curves; (b) The fitting to Duncan-Chang Model

The parameter E_i is called initial deformation modulus, which is an important parameter in Duncan-Chang Model. It's defined as:

$$E_i = \frac{1}{a} = 1 \Big/ \left(\frac{\varepsilon_1}{\sigma_1 - \sigma_3} \right)_{\varepsilon_1 \to 0} \tag{10}$$

Equation (10) shows that E_i is regardless of ε_1 but is related to confining pressure σ_3 which is:

$$E_i = KPa \left(\frac{\sigma_3}{Pa} \right)^n \tag{11}$$

Equation (11) is obtained by carrying regression analysis in the log-log plot. Equation (11) can be transformed to Eq. (12) which is linear in the log-log plot:

$$\lg \frac{E_i}{Pa} = \lg \left(K \frac{\sigma_3}{Pa} \right) = \lg K + n \lg \left(\frac{\sigma_3}{Pa} \right) \tag{12}$$

where *Pa* is the standard atmospheric pressure used to make physical quantity dimensionless; K, n are parameters shown in Fig. 3.

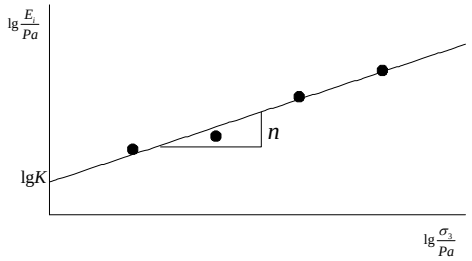

Fig. 3. The relationship between E_i and σ_3

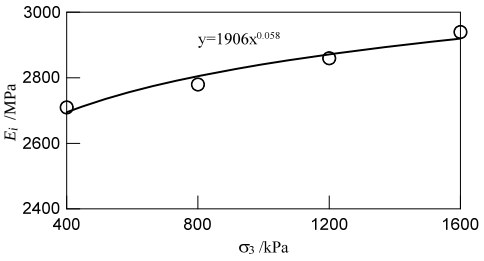

Fig. 4. E_i/Pa - σ_3/Pa curve

The initial deformation modulus of each confining pressure was calculated, and the data were fitted to Eq. (11). The fitting is shown in Fig. 4. As can be seen, the data match well with the Eq. (11).

From the above, it can be seen that confining pressure dependence can be reproduced in numerical conventional triaxial test with PFC2D.

3. Dilatation

The phenomenon of "dilatation" is common in granular materials such as incohesive soils, rockfill materials and so on. In such materials, "dilatation" is an important factor of the shear strength. Figure 5 shows the influence of "dilatation" on the shear strength. It's clear that "dilatation" depends on the density of materials, which is more obvious in the denser specimen.

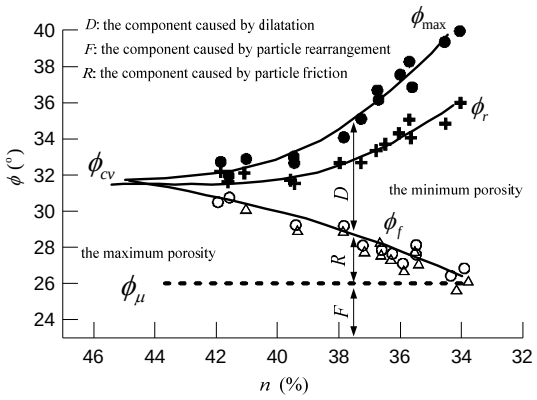

Fig. 5. The mechanism of shear strength of granular materials [34]

$\phi_{\max}$, the maximum friction angle; ϕ_r, the friction angle excluding dilatation [35]; ϕ_f, the friction angle excluding dilatation [36]; ϕ_{cv}, the friction when the volume is constant; ϕ_μ, the friction between particles

Rowe [37] developed a dilatancy equation from the particle level. Taking longitudinal compression as positive, and lateral expansion and instantaneous unit volume expansion, $\mathrm{d}\dot{V}/V$, positive, the equation is:

$$\frac{\sigma_1}{\sigma_3\left(1+\mathrm{d}\dot{V}/V\dot{\varepsilon}_1\right)}=\tan^2\left(45^\circ+\frac{1}{2}\phi_f\right) \tag{13}$$

or,

$$\frac{\sigma_1}{\sigma_3}=\tan^2\left(45^\circ+\frac{1}{2}\phi_f\right)\left(1+\mathrm{d}\varepsilon_v/d\varepsilon_1\right) \tag{14}$$

In the triaxial compression test, Eq. (14) becomes:

$$\frac{\sigma_1}{\sigma_3}=2\tan^2\left(45^\circ+\frac{1}{2}\phi_f\right)\left(-\frac{\mathrm{d}\varepsilon_3}{\mathrm{d}\varepsilon_1}\right) \tag{15}$$

In the biaxial compression test, Eq. (14) becomes:

$$\frac{\sigma_1}{\sigma_3}=\tan^2\left(45^\circ+\frac{1}{2}\phi_f\right)\left(-\frac{\mathrm{d}\varepsilon_3}{\mathrm{d}\varepsilon_1}\right) \tag{16}$$

where σ_1 is the major principal stress, ε_1 and ε_3 are the major principal strain and the minor principal strain respectively.

Assume $K_u=\tan^2\left(45^\circ+\frac{1}{2}\phi_f\right)$. Equation (14) shows that dilatation is related to $\frac{\sigma_1}{\sigma_3}$ and K_u. K_u depends on material properties and is regardless of the strain level, which is reflected in Fig. 6a. Figure 6a is the result of rockfill material in Pankou CFRD. As a result, K_u is a valid index for verifying the validity of PFC2D. Figure 6b confirms the above expection.

4. Nonlinearity and elastoplasticity

Unlike the materials such as metals, the stress-strain behaviors of granular materials are nonlinear. Elastoplasticity is another important behavior of granular materials. There is not only elastic deformation, but also plastic deformation. Figure 7 is one load cycle simulated with PFC2D. When unload is completed, there is still some deformation that is called plastic deformation. Also, hysteresis loops appear when reload is completed. Obviously, nonlinearity and elastoplasticity are reflected well.

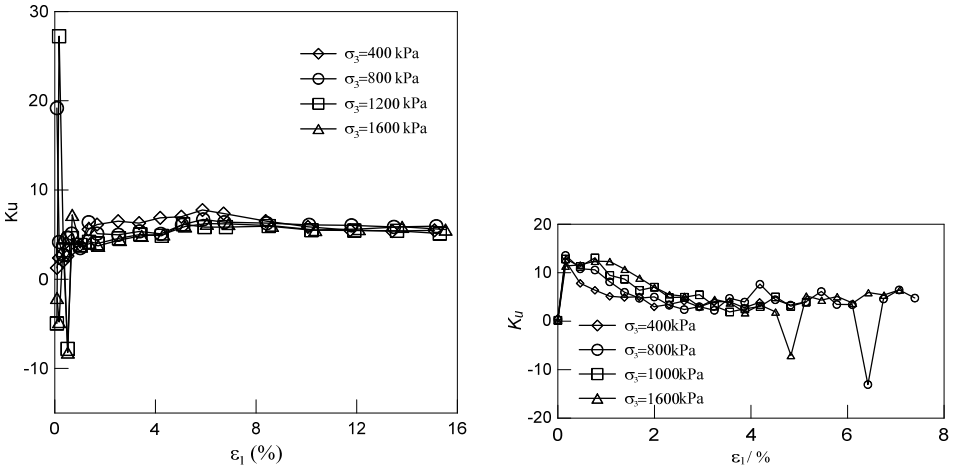

(a) (b)

Fig. 6. The dilatancy parameter K_u of Rowe Model

(a) the triaxial compression test of Pankou rockfill material; (b) the biaxial compression test of round particles

5. Strength criterion

Mohr-Coulomb strength criterion has been widely used to friction materials, which has been proved theoretically and physically. Coarse-grained materials are typical friction materials, so Mohr-Coulomb strength criterion is applicable, which is:

$$\tau = c + \sigma_3 \tan\varphi \tag{17}$$

where τ and σ_3 are shearing stress and normal stress respectively, c is cohesion, φ is friction angle.

Figure 8 is the Mohr-Coulomb stress circles achieved according to the conventional triaxial test simulated with PFC2D. In Fig. 8, c is equal to the intercept and φ is equal to the slope. We can see that the intercept c is almost zero and all the values of slopes are fluctuated in a small range, which can be considered as the constant φ. The results are consistent with Mohr-Coulomb strength criterion.

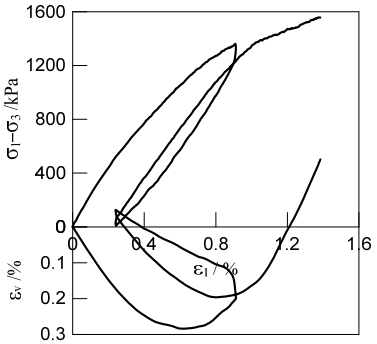

Fig. 7. Load-unload-reload stress-strain curve

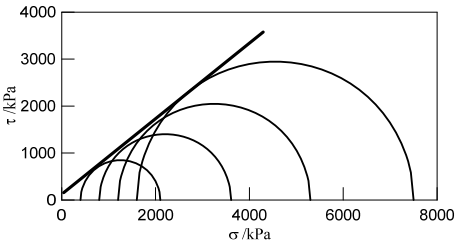

Fig. 8. Mohr-coulomb stress circle

6. Parameters of PFC2D

In PFC2D, parameters usually cannot be directly determined. The usual method is called *trial-and-error* calibration. The calibration process is as shown below: 1) the initial values of parameters are assumed; 2) simulate physical tests with PFC2D; 3) compare macroscopic responses of numerical tests with the responses of the matched physical tests. If the two responses are consistent, the initial values are right; if not, the initial values are inappropriate, thus, the values need to be changed; 4) repeat the above two steps until the right values are achieved.

Here the physical test is a conventional triaxial test. The material is spherical glass beads. There are two kinds of particle sizes which are 2mm and 22mm. The two kinds of particles are equivalent in terms of mass, that is, each mass percentage is 50%. The test instrument is large triaxial apparatus, which is 300mm in diameter. The physical parameters of the test are shown in Table 1 and the test results are shown in Fig. 9. From Fig. 9, we can see that the numerical test responses match well with the physical test responses, so the calibration process terminated. The final values of parameters are shown in Table 2. Besides, it should be mentioned that when the confining pressure is different, the values of parameters in PFC2D fluctuate slightly, which is inevitable in DEM simulation, and the values in Table 2 are the average values of the three confining pressures. Studies have showed that the parameter *K*n/*K*s is related to Poisson's ratio ν. An empirical formula is given as below:

$$Kn / Ks = 2(1+\nu) \tag{18}$$

Table 1. The physical parameters of the test

Diameter /(mm)	Void ratio *e*	Porosity *n*	Mass density ρ_s/(g/cm^3)	Dry density ρ_d/(g/cm^3)
2&22	0.346	0.257	2.41	1.79

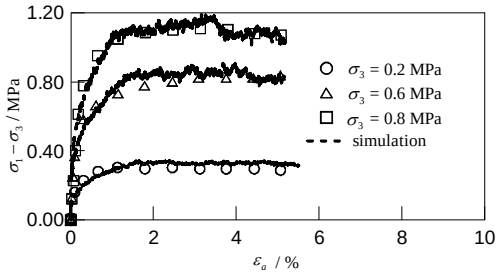

Fig. 9. Stress-strain curves of physical and numerical tests

Assume the value of Poisson ratio ν is 0.3. Then, the initial value of the parameter *Kn*/*Ks* is 2.60 according to Eq. (18) and the final value is 2.63. The final parameters in PFC2D are shown in Table 2.

Table 2. The values of parameters in PFC2D

Object	*Kn* / (N/m)	*Kn*/*Ks*	Mass density ρ_s /(g/cm^3)	Friction coefficient
Ball	5e9	2.63	2.70	0.6
Flexible wall	5e8	1.00	—	0.0
Rigid wall	5e10	1.00	—	0.0

b) Test program and process

In this section, the relative density tests were conducted by physical mode and numerical mode. The values of parameters are shown in Table 2. The purpose of the test is to get the maximum dry density and the minimum dry density. The test process is followed to the standard (Electic Power Press, 2006) [38].

1. Test program

The sample gradings were calculated from Eq. (7). The values of d_{max} are 40mm and 60mm. The values of *D* are 2.30, 2.40, 2.50, 2.55, 2.60 and 2.70. To make the relationship between the porosity and fractal dimension *D* clear, a numerical test program was added. The values of d_{max} are 60mm, 80mm, 100mm and 150mm, and the values of *D* are 1.90, 2.00, 2.10, 2.20, 2.30, 2.40, 2.50, 2.60, 2.70 and 2.75. The total amount of physical sample gradings is 2×6=12, and the number of numerical sample gradings is 4×10=40. The gradings are shown in Fig. 10. Each specimen was used to conduct two tests: the minimum dry density test and the maximum dry density test.

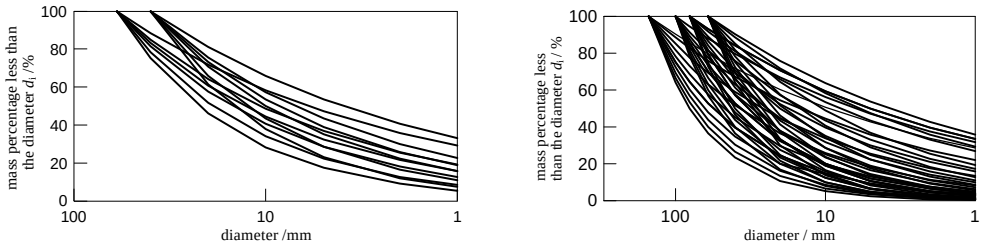

Fig. 10. The sample gradings
(a) The physical test; (b) The numerical test

2. Test process

2.1 The minimum dry density test

In the standard, the minimum dry density is obtained by the *loose-fill method*. The *loose-fill method* is described in the standard (Electic Power Press, 2006) [38]. The state of the minimum dry density is shown in Fig. 11a.

In PFC2D, the process is simulated as shown below: 1) generate numerical balls of the given mass in the tube which is 1.5 times larger than the tube given in the standard to guarantee that each ball has no contact with others; 2) make balls fall freely with the velocity of each ball being monitored. When any velocity of balls reaches one threshold, all velocities are made zero. The velocity threshold is determined as:

$$v = \sqrt{2gh} \tag{19}$$

where v is the velocity, g is acceleration of the gravity, h is the tolerated distance between the falling ball and the surface of balls in the tube. Here, h is 2cm according to the standard [38]; 3) calculate the volume of balls fallen into the cylinder. Then, the minimum dry density can be calculated easily. The numerical process is shown in Fig. 11b.

(a)

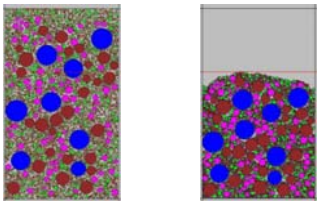

(b)

Fig. 11. The minimum dry density
(a) The physical process; (b) The numerical process

2.2 The maximum dry density test

The maximum dry density is achieved by *the surface-vibration method* given in the standard (Electic Power Press, 2006) [38]. The main parameters of the vibrator are frequency and centripetal force. The values of the two parameters are 45Hz-50Hz and 4.2kN-5.4kN respectively. The vibration time is 8min to guarantee that the specimen reaches the densest state. The vibrator and its parameters are shown in Fig. 12.

Fig. 12. The equipment used in the maximum density test

In PFC2D, the process is simulated as shown below: 1) the steel plate is simulated with a *clump* which is rigid comprised of some balls; 2) the vibration process is simulated by applying a sinusoidal force to the clump, which is mechanically equivalent to the vibration motor; 3) the size of the cylinder and the parameters of the vibrator are consistent with the standard (Electic Power Press, 2006) [38], and the vibration time is also 8 minutes. Figure 13 shows the physical process and numerical process of the maximum dry density test.

(a)

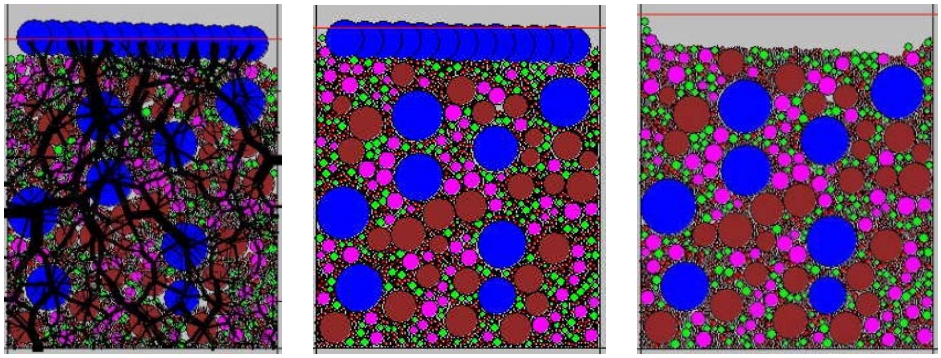

(b)

Fig. 13. The maximum density test
(a) The physical process; (b) The numerical process

c) Test results

The minimum dry density and the maximum dry density were translated to porosity n according to Eq. (20), and the results are shown in Table 3, 4 and Fig. 14.

$$n = 1 - \frac{\rho_d}{\rho_s} \tag{20}$$

From Fig. 14, we can see that the numerical results are consistent with the physical results on the whole, which verifies the numerical process. There are some similarities between the numerical results and the physical results as shown below: 1) the shape of the curves between porosity n and fractal dimension D; 2) the existence of the critical fractal dimension D_c; 3) D_c's independence of $d_{\max}$ and the relative density D_r. Of course, there are some differences: 1) the value of the porosity n with the same values of $d_{\max}$ and D; 2) the value of the critical fractal dimension D_c. From Table 3 and Table 4, the fact is clear that the values of porosity n in the physical tests are larger than the values in the numerical tests. The main reason is that the material is rockfill with complex shapes in the physical tests, but the material is ball in the numerical tests. Obviously, the ball is denser than non-spherical materials with the same compaction energy. The reason for the differences of the value of D_c is that particles whose diameters are smaller than 1mm are substituted with particles with the same diameters that are 1mm by quality equivalent in the numerical tests. However, particles whose diameters are smaller than 1mm are not sieved further in the physical tests. This means that the grading of these particles is consistent with the grading of original rockfills. Obviously, the two gradings are different, and the latter is better than the former, so particles whose diameters are smaller than 1mm in the physical tests are denser. As a result, in the numerical tests, the density of the fine particles (<1mm) is smaller than that in the physical tests. Thus, the phenomenon that the value of D_c in the physical tests is larger than the value in the numerical tests is interpretable, which means that more fine particles exist in the physical tests in the critical grading.

Table 3. The results of the relative density test in physical tests

$d_{\max}$ /(mm) \ D		2.30	2.40	2.50	2.55	2.60	2.70
40	$n_{\max}$	0.432	0.364	0.339	0.334	0.335	0.343
	$n_{\min}$	0.274	0.233	0.202	0.185	0.189	0.222
60	$n_{\max}$	0.379	0.354	0.320	0.316	0.318	0.329
	$n_{\min}$	0.272	0.227	0.187	0.178	0.181	0.193

Table 4. The results of the relative density test in numerical tests

$d_{\max}$ /(mm) \ D		1.90	2.00	2.10	2.20	2.30	2.40	2.50	2.60	2.70	2.75
60	$n_{\max}$	0.244	0.239	0.229	0.214	0.205	0.198	0.194	0.201	0.210	0.220
	$n_{\min}$	0.157	0.150	0.138	0.132	0.127	0.125	0.124	0.138	0.153	0.163
80	$n_{\max}$	0.243	0.238	0.226	0.212	0.201	0.193	0.186	0.191	0.199	0.208
	$n_{\min}$	0.156	0.146	0.133	0.126	0.119	0.116	0.115	0.127	0.140	0.150
100	$n_{\max}$	0.242	0.237	0.224	0.210	0.196	0.185	0.179	0.182	0.190	0.195
	$n_{\min}$	0.156	0.144	0.130	0.119	0.112	0.106	0.104	0.116	0.130	0.139
150	$n_{\max}$	0.240	0.234	0.223	0.206	0.187	0.176	0.172	0.175	0.180	0.185
	$n_{\min}$	0.156	0.140	0.126	0.114	0.104	0.099	0.097	0.106	0.121	0.129

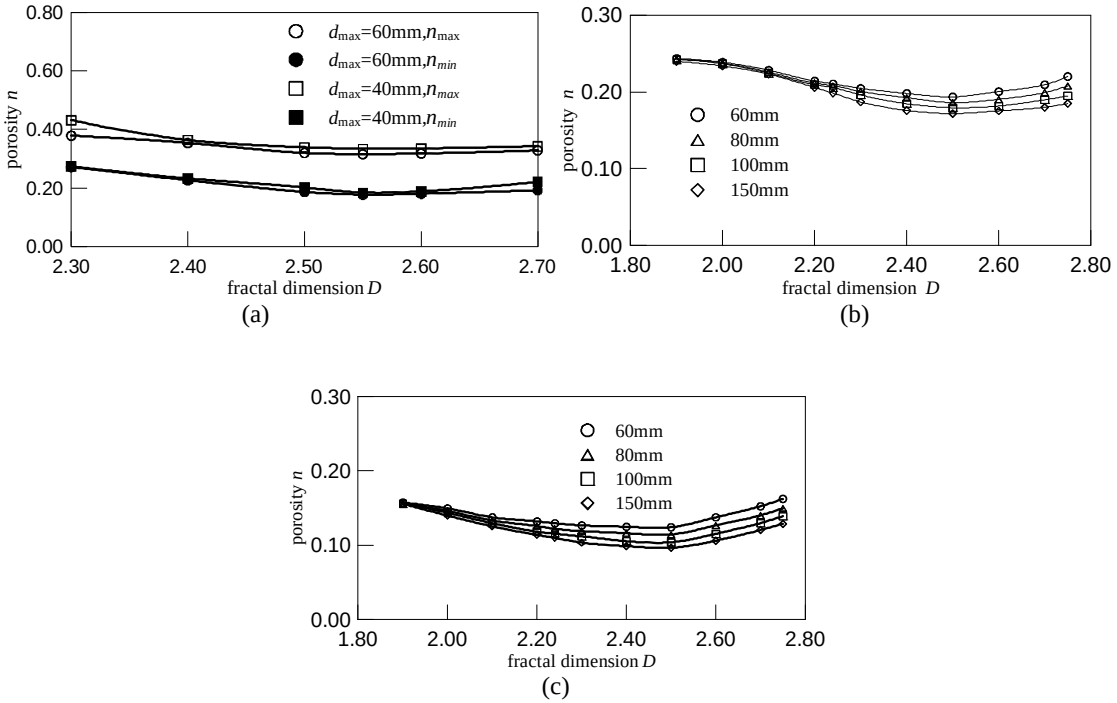

Fig. 14. The curves between porosity n and fractal dimension D

(a) The physical test; (b) The maximum porosity in numerical test; (c) The minimum porosity in numerical test

4. DISCUSSIONS

The most important feature of fractal theory is scale independence. This means that although the values of $d_{\max}$ are different, the gradings are similar only if fractal dimensions D are the same. Further, the densities should be the same according to the similarity criterion. However, Fig. 9 shows a discrepancy which indicates the densities are different and the differences are increasing with the growth of the value of fractal dimension D. The reasons are analyzed as shown below.

a) The scale independence feature in the grading

The grading calculated with Eq. (7) is considered to satisfy fractal theory. Two examples of such gradings were analyzed. The two gradings are shown in Table 5. The values of fractal dimension D are both 2.50 and the values of $d_{\max}$ are 200mm and 100mm respectively. The diameters of the grading II are half of the diameters of the grading I, but the corresponding mass percentages have the same value. This reflects scale independence of fractal theory. Further, there is another aspect which also reflects scale independence. For example, in the grading I, fractions of 20mm-40mm, 40mm-80mm and 80mm-200mm are 13.10%, 18.52% and 36.75% respectively. After reducing the fractions by 2 times, fractions become 10mm-20mm, 20mm-40mm and 40mm-100mm and the mass percentages are 9.26%, 13.10% and 25.99% respectively. It's obvious that 13.10%: 18.52%: 36.75% = 9.26%: 13.10%: 25.99% = 1.00: 1.41: 2.81. This is scale independence in another sense.

Table 5. Two example gradings

d_i /(mm) / p_i /(%)	200	160	120	100	80	60	40	20	10	5
I	100.00	89.44	77.46	70.71	63.25	—	44.72	31.62	22.36	—
II	—	—	—	100.00	89.44	—	63.25	44.72	31.62	22.36

b) Deviation analysis

According to scale independence in the grading, gradings with the same fractal dimension *D* should have the same physical and mechanical properties with the assumption that particle shapes are the same. Thus, the densities should be the same, but there are some differences of densities as shown in Fig. 14. In Fig. 14, we can see that though the values of fractal dimension *D* are the same, specimens are denser with the growth of d_{max}. It appears to conflict with scale independence. The reasons were discussed as below.

Scale independence is valid only if two conditions are satisfied: 1) the values of fractal dimension *D* are the same; 2) the diameters of two groups are proportional. As a result, Eq. (21) is satisfied. However, in the above test, the minimum diameters of all the gradings are 1mm, which does not agree with Eq. (21), so the condition 2) is not satisfied and scale independence becomes invalid.

$$\frac{d^1{}_{max}}{d^2{}_{max}} = \frac{d^1{}_{min}}{d^2{}_{min}} \quad \text{or} \quad \frac{d^1{}_{max}}{d^1{}_{min}} = \frac{d^2{}_{max}}{d^2{}_{min}} \tag{21}$$

Now, take D = 2.50 for example. Two groups of gradings were analyzed. One satisfies the conditions of scale independence and the other does not. In the former group, the values of d_{max} are 40mm, 80mm, 120mm and 160mm; the values of d_{min} are 1mm, 2mm, 3mm and 4mm. In the latter group, the values of d_{max} are 40mm, 80mm, 120mm and 160mm; the values of d_{min} are all the same. Obviously, in the former group, $\frac{d^1{}_{max}}{d^1{}_{min}} = \frac{d^2{}_{max}}{d^2{}_{min}} = \frac{d^3{}_{max}}{d^3{}_{min}} = \frac{d^4{}_{max}}{d^4{}_{min}}$ makes sense while in the latter group, it makes no sense. In the latter group, *truncation error* exists which is defined as $\delta = 100\left(p^2{}_1 - p^1{}_1\right)/\, p^1{}_1$, where $p^2{}_1$, $p^1{}_1$ are mass fractions whose diameters are smaller than 1mm. Figure 15 shows the results of the relative density tests of the two groups of gradings. The group without truncation error satisfies scale independence, so both the maximum porosities and minimum porosities are independent of diameters. However, the other group with truncation error doesn't satisfy it, so the porosities are dependent on diameters. The relationship between the changes of porosity and diameters is shown in Fig. 16. Figure 16 also shows the relationship between truncation error and diameters. We can see that all the curves can be approximately regarded as hyperbolas. The relationship between the changes of porosity and truncation error is shown in Fig. 17. A linearity relationship exists.

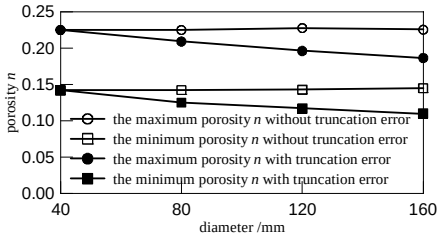

Fig. 15. The results of the relative density test and diameters

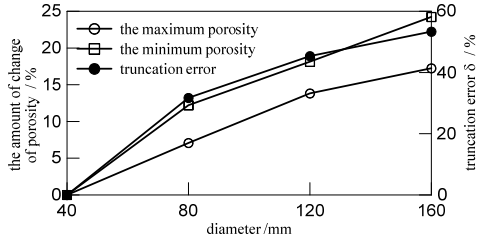

Fig. 16. The relations between deviations

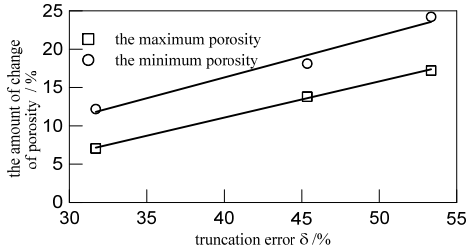

Fig. 17. The relation between the changes of porosity and truncation error

From the above, we can see that scale independence in densities must meet the two conditions shown before. However, in rockfill materials, particles whose diameters are smaller than 0.075mm are very few, so the minimum diameter can be approximately regarded as 0.075mm, which means that truncation error exists. As a result, scale independence isn't satisfied and the densities are not the same as shown in Fig. 14a.

c) Evaluation of the existing scale methods

There are four scale methods which are Exclusion Method, Similar Grading Method, Equivalent Substitution Method and Mixed method. The details of the four methods are shown in the standard (Electric Power Press, 2006) [38]. In this section, more attention was given to the relationship between scale method and fractal theory. According to the reference [32], most of the gradings of rockfills satisfy fractal grading, so an assumption was made that gradings appearing as shown below are all fractal gradings.

1. Exclusion method

The method is also called Full Quantity Substitution Method. The content of one fraction can be calculated with the following formula:

$$\Delta p_i = 100\Delta p_{0i} / \left(100 - P_{d\max}\right) \tag{22}$$

where Δp_i is one fraction of scaled grading; Δp_{0i} is one fraction of the original grading; $P_{d\max}$ is the content of oversized particles.

According to the assumption above, the original grading satisfies Eq. (7). So,

$$\Delta p_{0i} = p_i - p_{i+1} = 100\left[\left(\frac{d_i}{d_{\max}}\right)^{3-D} - \left(\frac{d_{i+1}}{d_{\max}}\right)^{3-D}\right] \tag{23}$$

where p_i is the mass percentage when $d \le d_i$. Here, assume that $d_i \ge d_{i+1}$.

Substitute Eq. (23) into Eq. (22):

$$\begin{aligned}\Delta p_i &= C\Delta p_{0i} = C(p_i - p_{i+1}) \\ &= C100\left[\left(\frac{d_i}{d_{\max}}\right)^{3-D} - \left(\frac{d_{i+1}}{d_{\max}}\right)^{3-D}\right]\end{aligned} \tag{24}$$

where $C = 1/(100\text{-}P_{d\max})$.

$$\begin{aligned}p_i &= \Delta p_i + \Delta p_{i+1} + \Delta p_{i+2} + \Delta p_{i+3} + \ldots\ldots + \Delta p_{i+\infty} \\ &= 100C\left[\left(\frac{d_i}{d_{\max}}\right)^{3-D} - \left(\frac{d_{i+\infty}}{d_{\max}}\right)^{3-D}\right] \\ &= 100C\left(\frac{d_i}{d_{\max}}\right)^{3-D} = 100\left(\frac{d_i}{\frac{d_{\max}}{C^{\frac{1}{3-D}}}}\right)^{3-D} \\ &= 100\left(\frac{d_i}{d'_{\max}}\right)^{3-D}\end{aligned} \tag{25}$$

$$C^{\frac{1}{3-D}} = \left[100/\left(100-P_{d\max}\right)\right]^{\frac{1}{3-D}}$$
$$= p_{d\max}^{\frac{-1}{3-D}} = \left(\frac{d'_{\max}}{d_{\max}}\right)^{(3-D)\left(\frac{-1}{3-D}\right)} = \left(\frac{d_{\max}}{d'_{\max}}\right) \tag{26}$$

where $d'_{\max}$ is the maximum diameter of the scaled grading.

Equation (25) shows that the scaled grading is also fractal grading. Further, the values of fractal dimension D are the same.

2. Similar Grading Method

The scaled grading is geometrically similar to the original grading, which is represented as:

$$n_r = \frac{d_{\max}}{d'_{\max}}, d_{ni} = \frac{d_{0i}}{n_r}, p_{ni} = p_{0i} \tag{27}$$

where n_r is the scale ratio; d_{0i} is the diameter of the original grading; d_{ni} is the diameter of the scaled grading; p_{0i} is the mass content when $d \le d_{0i}$; p_{ni} is the mass content when $d \le d_{ni}$.

Substitute Eq. (7) into Eq. (27), the following equation is obtained:

$$p_{ni} = p_{0i} = 100\left(\frac{d_{0i}}{d_{\max}}\right)^{3-D}$$
$$= 100\left(\frac{d_{ni}\times n_r}{d'_{\max}\times n_r}\right)^{3-D} = 100\left(\frac{d_{ni}}{d'_{\max}}\right)^{3-D} \tag{28}$$

From Eq. (28), we can see that the scaled grading is also fractal grading with the same value of fractal dimension D to the original grading.

3. Equivalent substitution method and mixed method

In Equivalent Substitution Method, the oversized particles are replaced in proportion by the particles whose diameters are smaller than $d'_{\max}$, and are more than 5mm. The content of one fraction is as shown below:

$$\Delta p_i = P_5 \Delta p_{0i} / \left(P_5 - P_{d\max}\right) \tag{29}$$

where P_5 is the mass content of the original grading when d>5mm.

Mixed Method is suggested by mixing Similar Grading Method and Equivalent Substitution Method. Both of the methods are based on the point that when the content of fine particles (d<5mm) is too much, the mechanical properties of the scaled grading are not consistent with those of the original grading any longer, so the content of fine particles must be limited to a reasonable extent.

In order to study the relationship between fractal theory and the above two methods, a formula was suggested as shown below:

$$p_i = A + \left(100 - A\right)\left(\frac{d_i}{d'_{\max}}\right)^{3-D} \tag{30}$$

where A is the parameter.

Given the value of p_5, A can be calculated by Eq. (30).

$$A=\frac{p_{5c}-100\left(\frac{5}{d'_{\max}}\right)^{3-D}}{1-\left(\frac{5}{d'_{\max}}\right)^{3-D}} \tag{31}$$

where p_{5c} is the content of fine particles pre-specified.

An example was taken to study the relationship between Eq. (30) and the two scale methods. The details are shown in Table 6. In Table 6, I, II, III and IV represent Equivalent Substitution Method, Eq. (30) I, Mixed Method and Eq. (30) II respectively. Table 6 shows that both Equivalent Substitution Method and Mixed Method can be reflected with Eq. (30) only if the contents of fine particles p_5 are the same.

Table 6. Gradings of different scale methods

d_i/(mm) / p_i/(%)	800	600	400	200	100	80	60	40	20	10	5
	100.00	89.13	75.79	57.43	43.53	39.81	35.48	30.17	22.87	17.33	13.13
I	—	—	—	—	—	—	100.00	79.35	50.96	29.44	13.13
II	*A* -37.91	*D* 2.60	—	—	—	—	100.00	79.35	50.96	29.44	13.13
III	—	—	—	—	—	—	100.00	80.35	53.33	32.85	17.33
IV	*A* -31.25	*D* 2.60	—	—	—	—	100.00	80.35	53.33	32.85	17.33

From the above, we can see that a close relationship exists between fractal theory and the four scale methods, which can be represented with a unified formula as shown below:

$$p_i=A+(100-A)\left(\frac{d_i}{d'_{\max}}\right)^{3-D} \tag{32}$$

In Exclusion Method and Similar Grading Method, the value of parameter A is zero and in Equivalent Substitution Method and Mixed Method, the value can be determined with Eq. (32).

5. CONCLUSION

Fractal theory was applied to the design of grading of rockfill materials and a formula was deduced. Then, to study the fractal properties of densities of rockfill materials, the physical and numerical relative density tests were conducted. Finally, some conclusions were determined:

(1) PFC2D can reflect the main mechanical properties of geotechnical materials, so it can be applied to simulate geotechnical problems.

(2) There are close relationships between fractal dimension and densities of rockfill materials. The densities are maximal when fractal dimension D is the critical value D_c. Further, D_c is independent of the relative density D_r and the maximum diameter $d_{\max}$.

(3) *Truncation error* is one of the main factors of scale effect of densities of rockfill materials, and there is a linear relationship between scale effect in terms of porosity and *truncation error*.

(4) The existing four scale methods in the standard can all be explained with fractal theory. A unified formula was suggested from the view of fractal theory, which is the basis for further studying scale effect of rockfill materials by fractal theory.

In this paper, several attempts were made to study the applicability of fractal theory to scale effect of rockfill materials. However, this is just the beginning of the study on scale effect. More efforts need to be made in the future to solve the scale effect of rockfill materials problem.

Acknowledgements: The Authors gratefully acknowledge the support of "Eleventh Five" National Science and Technology Support Project (2008BAB29B02).

REFERENCES

1. Yang, Z., Zhou, J., Jiang, G. & Sui Y. (2011). Development of concrete faced rockfill dam in China. *Water Power*, Vol. 37, No. 2, pp. 0018-0023(in Chinese).
2. Xu, Z. & Deng, G. (2008). Development of high CFRD and key technologies for building super-high CFRD. *Journal of Hydraulic Engineering*, Vol. 39, No. 10, pp. 1226-1234(in Chinese).
3. Hunter, G. & Fell, R. (2003). Rockfill modulus and settlement of concrete face rockfill dams. *Journal of Geotechnical and Geoenvironmental Engineering*, Vol. 129, No. 10, pp. 909-917.
4. Lee, J. Y., Choi, Y. K., Kim, H. S. & Yun, S. T. (2005). Hydrologic characteristics of a large rockfill dam: Implications for water leakage. *Engineering Geology*, Vol. 80, No. 1, pp. 43-59.
5. Yu, Y., Xie, L. & Zhang, B. (2005). Stability of earth–rockfill dams: influence of geometry on the three-dimensional effect. *Computers and Geotechnics*, Vol. 32, No. 5, pp. 326-339.
6. Deluzarche, R. & Cambou, B. (2006). Discrete numerical modeling of rockfill dams. *International Journal for Numerical and Analytical Methods in Geomechanics*, Vol. 30, No. 11, pp. 1075-1096.
7. Oldecop, L. A. & Alonso, E. A. (2007). Theoretical investigation of the time-dependent behavior of rockfill. *Géotechnique*, Vol. 57, No. 3, pp. 289-301.
8. Kim, Y. S. & Kim, B. T. (2008). Prediction of relative crest settlement of concrete-faced rockfill dams analyzed using an artificial neural network model. *Computers and Geotechnics*, Vol. 35, No. 3, pp. 313-322.
9. Bishop, W. A. & Henkel, D. J. (1948). *The measurement of soils properties in the triaxial test*. London: Edward Arnold ltd.
10. Marachind, N. D., Chan, C. K. & Seed, H. B. (1972). Evaluation of properties of rockfill materials. *Soil Mech. Found. Div.*, Vol. 98, No. 1, pp. 95-114.
11. Guo, Q. G. (1998). *The engineering properties and application of coarse-grained materials*. Zhengzhou: the Yellow River Water Press, (in Chinese).
12. Arabani, M. & Karami, M. V. (2007). A simple nonlinear-elastic model for prediction of lime stabilized clayey sand behavior. *Iranian Journal of Science & Technology, Transaction B, Engineering*, Vol. 31, No. B5, pp. 573-576.
13. Hardin, B. O. & Fellow, ? (1987). 1-D strain in normally consolidated cohesive soil. *Journal of Geotechnical Engineering, ASCE*, Vol. 113, No. 12, pp. 1449-1467.
14. Si, H. & Zhu, T. (1990). *Experimental study on rockfill materials in Xiao Langdi*. Nanjing: Hydraulic Research Institute, (in Chinese).
15. Ghanbarian, A. B., Sadeghpour, A. H., Mohamadzadeh, H. & Mohamadzadeh, M. (2008). An experimental study on the behavior of rockfill materials using large scale tests. *Electronic Journal of Geotechnical Engineering*, Vol. 13, No. 1, pp. 1-16.
16. Marsal, R. J. (1973). *Mechanical properties of rockfill*. In: embankment-Dam engineering, casagrande volum, New York: Wiley, pp. 109-200.
17. Ramamurthy, T. & Gupta, K. K. (1986). Response paper to how ought one to determine soil parameters to be used in the design of earth and rockfill dams. *Proc., Indian Geotech. Conf. New Delhi, India*, pp. 15-19.
18. Wang, J. (1994). Deformation properties and scale effect of coarse-grained material. *Chinese Journal of Geotechnical Engineering*, Vol. 16, No. 4, pp. 89-95(in Chinese).
19. Hannes, R. C. (1953). The strength of gravel in direct shear testing of soils. *Soil Mechanics Symposium.*

Moscow, pp. 678-685 (in Russian).
20. Li, Z. (2007). The experimental study on scale effect of Sand-and-gravel materials under dynamic load. *Nanjing: Hohai University*, (in Chinese).
21. Yang, G., Liu, H. & Chen, Y. (2009). Scale effect on dynamic deformation properties of rockfill materials. *Journal of Hydroelectric Engineering*, Vol. 28, No. 5, pp. 122-126 (in Chinese).
22. Weng, H. (2008). Experimental study on scale effect of coarse-grained materials. Nanjing: Hohai University, (in Chinese).
23. Shi, Y., Xiao, J. & Quan, S. (2010). Fractal model for prediction of effective hydrogen diffusivity of gas diffusion layer in proton exchange membrane fuel cell. *International Journal of Hydrogen Energy*, Vol. 35, No. 7, pp. 2863-2867.
24. Tang, H., Zhu, J., Xi, Z., Di, X., Wang, J. & Ao, Q. (2010). Impact factors of fractal analysis of porous structure. *Science China Technological Sciences*, Vol. 53, No. 2, pp. 348-351.
25. Ghanbarian, A. B., Millán, H. & Huang, G. (2011). A review of fractal, prefractal and pore-solid-fractal models for parameterizing the soil water retention curve. *Canadian Journal of Soil Science*, Vol. 91, No. 1, pp. 1-14.
26. Huang, J. & Xun, Y. (2012). Relationship of high-temperature performance and aggregate gradation of asphalt mixtures based on fractal theory. *Applied Mechanics and Materials*, Vol. 204, No. 1, pp. 3795-3798.
27. Ochiai, M., Ozao, R. & Yamazaki, Y. (1992). Self-similarity law of particle size distribution and energy law in size reduction of solids. *Physica A: Statistical Mechanics and its Applications*， Vol. 191, No. 4, pp. 295-300.
28. Tripathi, S. K., Kushwaha, C. P. & Basu, S. K. (2012). Application of fractal theory in assessing soil aggregates in Indian tropical ecosystems. *Journal of Forestry Research*, Vol. 23, No. 3, pp. 355-364.
29. Rakhshandehroo, G. R. & Ghadampour Z. (2011). A combination of fractal analysis and artificial neural network to forecast groundwater depth. *Iranian Journal of Science & Technology, Transactions of Civil and Environmental Engeering*, Vol. 35, No. C1, pp. 121-130.
30. Turcotte, D. L. (1986). Fractals and fragmentation. *Journal of Geophysical Research*, Vol. 91, No. B2, pp. 1921-1926.
31. Tyler, S. W. & Stephen, W. (1989). Application of fractal mathematics to soil water retention estimation. *Soil Science Society of America Journal*, Vol. 53, No. 4, pp. 987-996.
32. Yang, P., Luo, Y. & Shi, Y. (1993). The soil fractal properties of soil aggregate-size distributions calculated by mass. *Chinese Science Bulletin*, Vol. 38, No. 20, pp. 1896-1899 (in Chinese).
33. Zhu, S., Feng, Y. M., Feng, S. R. & Chen, W. Y. (2012). Particles gradation optimization of blasting Rockfill based on fractal theory, Wuhan: Advanced research on material engineering, architectural engineering and information. *Advanced Materials Research*, No. 366, pp. 469-473.
34. Tyler, S. W. & Wheatcraft, S. W. (1990). Fractal processes in soil water retention. *Water Resources Research*, Vol. 26, No. 5, pp. 1047-1054.
35. Wang, Y., Ren, J., Wu, L., Deng, Y. & Liang, X. (2012). Research on effectiveness of PFC used in simulating coarse-grained material properties. *Water Resources and Power*, Vol. 30, No. 10, pp. 0072-0075 (in Chinese).
36. Soil Engineering Society of Japan (1999). *Field compaction of coarse-grained materials*. Beijing: China WaterPower Press, (translated in Chinese).
37. Skempton, A. W. & Bishop, A. W. (1950). The measurement of the shear strength of soils. *Geotechnique*, Vol. 2, No. 2, pp. 90-108.
38. Newland, P. L. & Allely, B. H. (1957). Volume Changes in Drained Taixial Tests on Granular Materials. *Geotechnique*, Vol. 7, No. 1, pp. 17-34.
39. Rowe, P. W. (1962). The stress-dilatancy relation for static equilibrium of an assembly of particles in contact. *Proceedings of the Royal Society of London. Series A. Mathematical and Physical Sciences*, Vol. 269, No. 1339, pp. 500-527.
40. Electic Power Press, (2006). Code for coarse-grained soil tests for hydropower and water conservancy engineering. Beijing: China Electic Power Press, (in Chinese).